



Changes in the photosynthetic apparatus and lipid droplet formation in *Chlamydomonas reinhardtii* under iron deficiency

Elsinraju Devadasu¹ · Dinesh Kumar Chinthapalli^{1,3} · Nisha Chouhan¹ · Sai Kiran Madireddi¹ · Girish Kumar Rasineni² · Prabhakar Sripadi³ · Rajagopal Subramanyam¹

Received: 22 April 2018 / Accepted: 28 August 2018 / Published online: 14 September 2018
© Springer Nature B.V. 2018

Abstract

The unicellular photosynthetic alga *Chlamydomonas reinhardtii* was propagated in iron deficiency medium and patterns of growth, photosynthetic efficiency, lipid accumulation, as well as the expression of lipid biosynthetic and photosynthesis-related proteins were analysed and compared with iron-sufficient growth conditions. As expected, the photosynthetic rate was reduced (maximally after 4 days of growth) as a result of increased non-photochemical quenching (NPQ). Surprisingly, the stress-response protein LHCSR3 was expressed in conditions of iron deficiency that cause NPQ induction. In addition, the protein contents of both the PSI and PSII reaction centres were gradually reduced during growth in iron deficiency medium. Interestingly, the two generations of Fe deficiency cells could be able to recover the photosynthesis but the second generation cells recovered much slower as these cells were severely in shock. Analysis by flow cytometry with fluorescence-activated cell sorting and thin layer chromatography showed that iron deficiency also induced the accumulation of triacylglycerides (TAG), which resulted in the formation of lipid droplets. This was most significant between 48 and 72 h of growth. Dramatic increases in DGAT2A and PDAT1 levels were caused by iron starvation, which indicated that the biosynthesis of TAG had been increased. Analysis using gas chromatography mass spectrometry showed that levels of 16:0, 18:0, 18:2 and 18:3^{Δ9,12,15} fatty acids were significantly elevated. The results of this study highlight the genes/enzymes of *Chlamydomonas* that affect lipid synthesis through their influence on photosynthesis, and these represent potential targets of metabolic engineering to develop strains for biofuel production.

Keywords Electron transport · Iron deficiency · LHCSR3 · Major lipid droplet protein · Photosystems · Triacylglycerol

Electronic supplementary material The online version of this article (<https://doi.org/10.1007/s11120-018-0580-2>) contains supplementary material, which is available to authorized users.

✉ Rajagopal Subramanyam
srgsl@uohyd.ernet.in

¹ Department of Plant Sciences, School of Life Sciences, University of Hyderabad, Hyderabad, Telangana 500046, India

² Center for Excellence in Medical Services Pvt. Ltd., Kineta Towers, Road No. 3, Banjara Hills, Hyderabad, Telangana 500034, India

³ Analytical Chemistry and Mass Spectrometry, CSIR-Indian Institute of Chemical Technology, Hyderabad, Telangana 500 007, India

Introduction

The microalgae, a diverse group of eukaryotic photosynthetic organisms, occupy diverse habitats including freshwater, marine and more extreme environments such as hot springs and frozen regions (Li et al. 2012a, b). This ability to adapt to different environmental conditions is due to the plasticity of algal physiology. Microalgae have been used as a source of biodiesel (Chisti et al. 2007) and they are considered promising candidates for large-scale biofuel production due to their high photosynthetic efficiency and oil accumulation ability (Borowitzka and Moheimani 2013; Moody et al. 2014).

Abiotic stress leads to a variety of cellular responses in eukaryotic photosynthetic algae, including changes to the photosynthetic apparatus (Glaesener et al. 2013). In addition, stress leads to increased accumulation of lipids, particularly triacylglycerides (TAG) (Juergens et al. 2015).

Lipid accumulation is thought to help microalgae withstand adverse environmental conditions (BenMoussa-Dahmen et al. 2016). Nitrogen starvation, which is normally detrimental to algal growth, was found to cause increased TAG accumulation and lipid droplet formation (James Gabriel et al. 2011). Another abiotic stress, salinity, was also shown to significantly enhance the synthesis of neutral lipids, specifically TAG. The limitation of micronutrients (e.g. zinc and iron) can result in the alteration of membrane lipids and the formation of lipid droplets (Chen et al. 2011). In conditions of iron and zinc deprivation, the growth of *D. tertiolecta* is severely inhibited and the cells accumulate neutral lipids (Chen et al. 2011; Urzica et al. 2013). Microalgae have two iron-rich organelles: the chloroplast and mitochondrion. Both organelles contain numerous iron-dependent proteins whose functions are essential in electron transfer pathways. An inadequate supply of iron limits the photosynthetic process leading to lipid accumulation (Glaesener et al. 2013).

The unicellular green microalgae, *Chlamydomonas* (*C.*) *reinhardtii*, is a model organism that has been used in the study of basic physiology and for investigating the regulation of primary metabolism (Merchant et al. 2007). It is genetically well characterized and displays a significant response to adverse conditions, so it was chosen as a suitable organism to investigate changes in lipid metabolism caused by iron deficiency. According to the current model, TAG accumulation in *C. reinhardtii* and related species occurs in the endoplasmic reticulum (ER), plastids, and at contact site between plastids and the ER (Fan et al. 2011). The final step of TAG biosynthesis is catalysed by diacylglycerol acyltransferase (DGAT), which transfers an acyl group to sn-1,2-diacylglycerol (DAG). *Chlamydomonas* has at least two types of DGAT that use acyl-CoA as the acyl donor: type I represented by DGAT1 and type II represented by DGTT1–DGTT5 (Boyle et al. 2012). Another type of acyltransferase, phospholipid:diacylglycerol acyltransferase 1 (PDAT1), transfers acyl groups from a wide range of glycerolipids to TAG (Yoon et al. 2012). Recently, monogalactosyldiacylglycerol (MGDG), a signature lipid class of photosynthetic membranes, was identified as a plastidic source of certain acyl groups in TAG biosynthesis (Li et al. 2012a, b). The mechanism of lipid biosynthesis in *C. reinhardtii* and the genes/proteins involved have not been extensively studied under Fe deficiency. Moreover, little is known about their expression under stress conditions such as micro-nutrient deficiency. Due to its potential influence on TAG accumulation, iron deprivation stress is likely to have wide-ranging effects not only on iron-rich organelles like chloroplasts and mitochondria but also on ER and membrane structures.

Under iron-deficient conditions, photosynthetic eukaryotes become chlorotic and their plastids are often smaller and less well developed (Moseley et al. 2002). The abundance of photosynthetic machinery is decreased due to

chlorosis, which is preceded by structural remodelling of photosystems (PS) I and PSII (Moseley et al. 2002; Busch et al. 2008; Yadavalli et al. 2012a; Devadasu et al. 2016). In higher plants, the greatly decreased level of photosynthetic proteins also alters electron transport in PSII and PSI (Andaluz et al. 2006; Timperio et al. 2007; Msilini et al. 2011; Chen et al. 2015). In cyanobacteria deprived of iron, the light-harvesting phycobilisomes were reduced and an iron-stress-induced operon *isiAB* is expressed (Bibby et al. 2001; Boekema et al. 2001). Iron stress-induced protein A (IsiA) displays homology to CP43, a chlorophyll *a*-binding protein of PSII. A ring of 18 molecules of IsiA forms around the PSI trimeric reaction centers (Bibby et al. 2001; Boekema et al. 2001). Another report states that two centric layers of IsiA form around trimeric PSI following prolonged growth in nanomolar Fe levels (Chauhan et al. 2011). In addition, the major effect of iron deprivation has been reported to be monomerization of the PSI trimers of whole cells *in vivo*, but not the formation of IsiA ring around the PSI trimers. This is quite spectacular as observation, but represent only a small fraction of the PSI reaction centers under iron-limited conditions (Ivanov et al. 2006).

In conditions of Fe deficiency, the PSI-associated light-harvesting complex I (PSI-LHCI) of *C. reinhardtii* undergoes remodelling which results in a decreased PSI antenna size (Naumann et al. 2005, 2007). These structural changes decrease the efficiency of excitation energy transfer between LHCI and PSI. PSII is also damaged by iron deprivation but to a lesser extent than PSI (Yadavalli et al. 2012a; Devadasu et al. 2016). Iron stress also induces TAG accumulation and lipid droplet formation in *C. reinhardtii*. In this study, *C. reinhardtii* was subjected to progressive iron deficiency conditions in order to understand the changes induced in photosynthetic efficiency and lipid metabolism. Furthermore, TAG accumulation and lipid droplet formation under iron stress were explored and the expression of key genes/enzymes connected with photosynthesis efficiency was studied.

Materials and methods

Culture and growth conditions

Chlamydomonas reinhardtii CC125 wild-type (*wt*) and the mutant strain NPQ4 (*npq4*) were obtained from the *Chlamydomonas* resource centre (<http://www.chlamy.org/>). Cells were grown photoheterotrophically in Tris-acetate phosphate medium at 25 °C with a photon flux density of 50 $\mu\text{mol photons m}^{-2} \text{s}^{-1}$ in 250-mL conical flask shaken at 120 rpm in an orbital shaker (Terauchiet al. 2010; Yadavalliet al. 2012a).

Iron starvation time course

To induce iron starvation, cells (*wt* and *npq4*) were grown to mid-logarithmic phase (3×10^6 cells mL⁻¹), then collected by centrifugation (3000 rpm for 5 min at RT) and washed three times in Fe-less TAP medium. The cell suspensions were then used to inoculate 500 mL lots of Fe-less TAP medium in 1-L conical flasks. Cultures were incubated as described above and samples were collected at 0, 12, 24, 48, and 72 h. Parallel cultures were grown in standard TAP medium and samples were taken according to the same schedule as controls for subsequent analysis. Further, 50 mL of Fe deficiency cells [first generation of Fe deficiency (1st batch)] was centrifuged and these cells were again inoculated to the same amount of Fe deficiency [2nd generation of Fe deficiency (2nd batch)] medium (50 mL) and allowed them to grow up to 5–6 days. Similarly, the first and second generation of Fe deficiency cells were centrifuged and inoculated to the same amount of Fe containing medium and allowed them to recover till 5–6 days.

Biomass determination

For total biomass determination, 5 mL of the +Fe and –Fe cultures were collected after 72 h incubation and centrifuged in weighed tubes at 3000×g for 5 min. The pelleted cells were washed once with distilled water and then lyophilized at 4 °C for 8 h. The tubes were then weighed again and the total dry masses calculated.

Nile Red staining and microscopy

Samples collected from the cultures at 0, 12, 24, 48 and 72 h of incubation were immediately mixed with iodine solution (5 µL; 0.25 g Iodine in 100 mL of 95% ethanol) to immobilize the cells. The cell suspensions were then stained with Nile Red (NR) (1 µg mL⁻¹ final concentration, Sigma). Staining was performed in darkness for 20 min at room temperature with constant gentle agitation. The cells were then concentrated by centrifugation at 500×g for 3 min. Fluorescence and transmission images of the stained cells were acquired using a Zeiss LSM 8 PASCAL confocal microscope system with PASCAL version 4.0 software. The microscope was fitted with LASOS HeNe 543 nm and Argon 488 nm scanning lasers. Scans of the algal cells were taken with a ×60 objective at a pixel resolution of 1024×1024 in 8-bit format (pixel intensity range 0–255). Laser transmission and scan settings remained constant in all scans. Leica confocal software was used for image analysis.

Chlorophyll *a* OJIP fluorescence measurements

Chlorophyll *a* fluorescence fast induction curves (O–J–I–P) were measured using a plant efficiency analyzer (PEA, Hansatech, Kings Lynn, Norfolk, UK). The cells were dark adapted for 20 min and then exposed to a photon flux density of 3000 µmol photons m⁻² s⁻¹ produced by an array of three light-emitting diodes peaking at 650 nm.

Pulse amplitude modulated (PAM) fluorescence measurements

Culture samples were adjusted to a density of 3×10^6 cells mL⁻¹ and dark adapted for 20 min before fluorescence measurement performed using a pulse amplitude modulated 101 fluorometer (Walz GmbH, Effeltrich, Germany) connected to a PAM Data Acquisition System 100 controlled by PAM WINCONTROL v2.08 software (Heinz Walz GmbH, Effeltrich, Germany). The maximum potential quantum efficiency of PSII [$F_v/F_m = (F_m - F_o)/F_m$] was assessed after 20 min of dark incubation. Subsequently fluorescence rapid light curves (RLCs) were obtained using eight different actinic light intensities (Kosourov et al. 2007) (145, 221, 344, 536 and 830 µmol photons m⁻² s⁻¹ for 30 s each). Subsequently, the actinic light (250 µmol photons m⁻² s⁻¹) was maintained for 5 min, before a final saturating pulse was applied. The fluorescence rapid light curve (RLC) parameters were calculated according to Kosourov et al. (2007). Similarly, the Chlorophyll *a* fluorescence measurements were carried out from Handy PEA and PAM fluorescence for two generations of Fe deficiency cells and also from recovery for both generations of Fe sufficient cells.

Quantification of photosynthetic pigments and carotenoids

After 72-h growth, cultures of *C. reinhardtii* at a cell density of approx. 3×10^6 cells mL⁻¹ were harvested by centrifugation. The cell pellets were resuspended in 80% acetone and held for 20 min in the dark at –20 °C to extract the pigments. Total chlorophyll was estimated according to the method of Porra et al. (1989). For the estimation of total carotenoids, an equivalent number of cells were resuspended in 95% ethanol and held for 4 h in the dark at 4 °C. The extracts were then centrifuged and total carotenoids in the clarified supernatants were determined by measuring the optical density at 470 nm as previously described (Wellburn 1994).

Nile Red fluorescence assay for triacylglycerides (TAG)

The *C. reinhardtii* cultures were diluted to a density of 3×10^6 cells mL⁻¹ and placed in the wells of a 96-well

microplate. To each well, a 5 μL aliquot of 50 $\mu\text{g mL}^{-1}$ Nile Red (NR; Sigma; prepared in acetone) was added, mixed in by agitation and the plate incubated in the dark for 20 min. The neutral lipids were then measured by fluorescence (excit. 485 nm/emiss. 595 nm) using a plate reader (Tecan infinite 200, Magellan). Quantification was achieved using a standard curve prepared with the lipid Trioleine (Sigma T4792).

FACS analysis of neutral lipids

To further quantify neutral lipids stained with Nile Red, the fluorescence intensity was measured by flow cytometry. A 10 μL aliquot of 100 $\mu\text{g mL}^{-1}$ NR in acetone was added to 3.0×10^6 cells in 1 mL of TAP medium, gently mixed in and the tube held in the dark for 30 min. The cells were then harvested by centrifugation and resuspended in a small volume. Flow cytometry analysis was performed using a FACS Calibur Flow Cytometer (BD Falcon, USA) fitted with a 488-nm excitation filter and a 545-nm emission filter. Ten thousand cells were analysed without gating and auto fluorescence (from chlorophyll) was nullified before measuring the NR fluorescence. The fluorescence of NR was plotted on both dot plot and histogram.

Neutral lipid extraction and TLC analysis

The identification of TAG was performed by thin layer chromatography. To extract lipids, a 5-mg sample of lyophilized biomass was resuspended in a mixture of methanol, chloroform and 88% formic acid (2:1:1) plus 0.9% KCl (Andaluz et al. 2006). After vortexing to mix, the homogenate was centrifuged at $3000 \times g$ for 5 min to cause a phase separation. The organic layer was transferred to a clean glass tube and evaporated by nitrogen gas purging. The dried extract was then dissolved in 50 μL chloroform. As a standard for TAG identification, Triolein (Sigma-Aldrich) was dissolved in CHCl_3 for mg mL^{-1} concentration. The samples or Triolein standard (10 μL) were applied to silica gel plates by spraying using a Linomate 5 (Camag). The TLC plates were then run in a chamber filled with a mixture of petroleum ether–diethyl ether–acetic acid (80:20:1) for 20 min. Bands were visualized by brief staining with iodine.

Gas chromatography–mass spectrometry analysis

For extraction of lipids, the procedure is same as that of extraction procedure for TLC analysis. Extracted fatty acids were converted to their corresponding methyl esters by treatment with diazomethane (Cakmak et al. 2014). Heptadecanoic acid (C17:0) was added to samples as an internal standard during derivatization for both full scan and selected ion monitoring (SIM) mode analysis. Fatty acid methyl

esters (FAMES) were analysed by Gas Chromatography with an Electron Impact Mass Spectrometry (GC-EIMS) Agilent 7890B gas chromatograph (Agilent Technologies, Palo Alto, CA) equipped with a 5977A mass selective detector. An AB-5MS capillary column (length 30 m, i.d. 0.25 mm, film thickness 0.25 μm) was used for chromatographic separation. Samples of 1 μL were injected into the GC–MS instrument in split less mode. The GC oven was programmed to hold the temperature at 50 $^\circ\text{C}$ for 2 min followed by a 10 $^\circ\text{C min}^{-1}$ temperature ramp to 210 $^\circ\text{C}$. After a 1 min hold at 210 $^\circ\text{C}$, there followed a 2 $^\circ\text{C min}^{-1}$ ramp to 220 $^\circ\text{C}$ with a 2 min hold, and then a 10 $^\circ\text{C min}^{-1}$ ramp to 280 $^\circ\text{C}$ with a 2-min hold. Helium was used as the carrier gas in constant flow mode at a flow rate of 1 mL min^{-1} . The inlet and GC–MS interface temperatures were maintained at 250 $^\circ\text{C}$ and 280 $^\circ\text{C}$, respectively. The solvent delay time was set to 4 min. The EI source and quadrupole temperatures were maintained at 230 $^\circ\text{C}$ and 150 $^\circ\text{C}$, respectively. The mass spectrometer was scanned from m/z 29 to 600 for a full scan and SIM analysis. All fatty acid methyl esters (FAME) were identified and confirmed by NIST-Wiley library. FAME were further quantified by SIM mode analysis of specific ions m/z 74, m/z 87, for saturated and monoenoic acids, as well as m/z 79 and m/z 81 for FAMES having more than one double bond.

Protein identification by immunoblotting

Chlamydomonas reinhardtii cells were resuspended in SDT lysis buffer (4% SDS and 0.1 M DTT in 0.1 M Tris–HCl, pH 7.6), vortexed for 2 min and incubated at 95 $^\circ\text{C}$ for 5 min. The lysates were further centrifuged at $14,000 \times g$ for 10 min at room temperature and the supernatant transferred to a fresh tube. The total protein in each supernatant was quantified using the Bradford method (Bio-Rad) and samples containing 20 μg of protein were analysed by polyacrylamide gel electrophoresis (PAGE) using 10% or 15% Bis-Tris gels for DGAT2A and PDAT1, or 12% SDS gels for other proteins. Using a standard methodology (Towbin et al. 1979), the separated proteins were then transferred to nitrocellulose membrane, incubated with primary antibodies, and specific binding was disclosed. Specific primary antibodies (at different dilutions) were used to detect photosynthetic proteins: PsaA (1:2000), PsbA (1:5000), Rubisco small subunit, SSU (1:1000), and LHCSR3 (1:1000). Other antibodies were used to evaluate the expression patterns of acyl-CoA:diacylglycerol; acyltransferase (DGAT2A, 1:1000) and phospholipid:DAG acyltransferase (PDAT1, 1:250) (Boyle et al. 2012). An antibody against Histone H3 (1:5000) was used to confirm equivalent loading of the gels and efficient protein transfer to the membrane. The identification of major lipid-droplet protein (MLDP) was performed using an antibody (1:250) provided by Anthony H.C. Huang, USA.

All other primary antibodies were obtained from Agrisera (Sweden). The secondary antibody anti-chicken (1:10000) was used for identification of PsbA (Agrisera) and anti-rabbit (1:10000) was used for identification of other proteins (Cell Signalling Technology). Immunoblot images were obtained using a Chemidoc-touch imaging system (Bio-Rad).

Results

Growth characteristics and pigment analysis

To study the impact of iron deficiency on cell growth and structure, as well as on the photosynthetic apparatus, *C. reinhardtii* cells were propagated in iron-sufficient (control) and iron-deficient TAP medium. Growth curves were plotted by monitoring the change in A_{750} of the cultures (Supplementary Fig. 1). In the iron-sufficient conditions, the absorbance value increased twofold after 2 days and then reached a plateau at approximately 72 h. Similarly, the absorbance of the iron-deprived culture doubled over the first 2 days in culture but then it decreased to approximately half of the maximum value over the following 4 days. Notably, the cells grown in iron-deficient (– Fe) condition grew considerably slower in comparison to the control (+ Fe) cells. Further the second generation of Fe deficiency cells were grown very slowly (more than 6 days) than the first generation. These cells were centrifuged and re-inoculated to Fe sufficient medium to observe the recovery. In second generation cells, the recovery took place longer (more than 6 days) (data not shown). This difference in growth rate highlighted the importance of iron nutrition to *Chlamydomonas* cell growth.

To determine the effect of iron deficiency on the level of pigments associated with photosynthetic complexes of *C. reinhardtii*, total chlorophyll and pigment levels were quantified. Total chlorophyll levels were reduced by around 50% in iron-deprived cells compared with iron-sufficient cells (Supplementary Fig. 2a). The recovery also followed with growth pattern that the second generation cells accumulated the Chl to the control level after 6–7 days, whereas the first generation recovery was faster (Supplementary Fig. 2b). A change in the level of total carotenoids was also observed (data not shown). It has previously been shown that during iron starvation the membrane lipids of chloroplasts are remodelled and the levels of photosynthetic pigments and proteins are decreased in *C. reinhardtii* (Yadavalli et al. 2012a; Urzica et al. 2013). The degradation of the photosynthetic apparatus and decreased protein turnover are common metabolic changes that occur during iron deprivation. Our results confirm the importance of iron as an essential micro-nutrient for growth and chlorophyll biosynthesis in *C. reinhardtii*.

Chlorophyll *a* fluorescence analysis

Chl *a* fluorescence induction curves were used to monitor several photosynthetic events in *C. reinhardtii* strains (*wt* and *npq4* mutant) grown under Fe deficiency. When measured under saturating light Chl *a* fluorescence induction curves show a fast multiphasic rise occurring within the μ s to second(s) range known as the O–J–I–P transients (Kodru et al. 2015). In dark-adapted *C. reinhardtii* cells, it was shown that Q_A , an electron acceptor of PS II, is in the oxidized state at the O transient (the initial, minimum fluorescence). The O–J fluorescence rise (J is an inflection between O and the peak P) is a photochemical phase which is relevant to the reduction of Q_A to Q_A^- , whereas J–I (I being a second inflection between O and P) and I–P are thermal phases involving the reduction of the PQ pool (Stirbet and Govindjee 2011, 2012) as well as that of the electron acceptor side of PS I (Schansker and Strasser 2005; Kodru et al. 2015). As in our previous report (Kodru et al. 2015), typical OJIP curves were obtained from *wt* and the *npq4* mutant *C. reinhardtii* strains. In the cells grown under Fe deficiency (4 days), the O phase (initial fluorescence, F_0) was increased in the *wt*, whereas in the *npq4* mutant it was reduced. Furthermore, the OJ, JI and P phases were shorter in both strains grown in iron-deficient conditions, although this truncation was more drastic in the *npq4* mutant (Fig. 1a, c). Normalization of the fluorescence curves at O and P indicated that the changes occurred equally in all phases (Fig. 1b). In addition the components of fluorescence, F_m and F_v/F_m were drastically changed in both *wt* and *npq4* mutant under iron deficiency. The substantial reduction in the F_m value in the mutant indicated that non-photochemical quenching is very important in protection against Fe deficiency. From Fe deficiency, OJIP curves show that there was dramatic change in photosynthetic efficiency but still the cells were showing significant photosynthetic activity. In order to understand the severity of the Fe deficiency on cells, the cells grown under Fe deficiency were re-inoculated to Fe deficiency medium. After 6 days of growth, the photosynthesis efficiency was drastically reduced when compared to the first generation of Fe deficiency. We know that the first generation of Fe deficiency cells could recover the photosynthetic activity to the control cells after 4 days (Devadasu et al. 2016), whereas the second generation cells restored the photosynthetic activity after 6–7 days (Fig. 1f, g). It is interesting to note that both generations of Fe deficiency cells were in shock but they were alive.

Photosynthetic efficiency

Photosynthetic parameters were recorded for the cells grown from iron-sufficient and iron-deficient conditions (Fig. 2). Notably, the electron transport rate (ETR) decreased faster

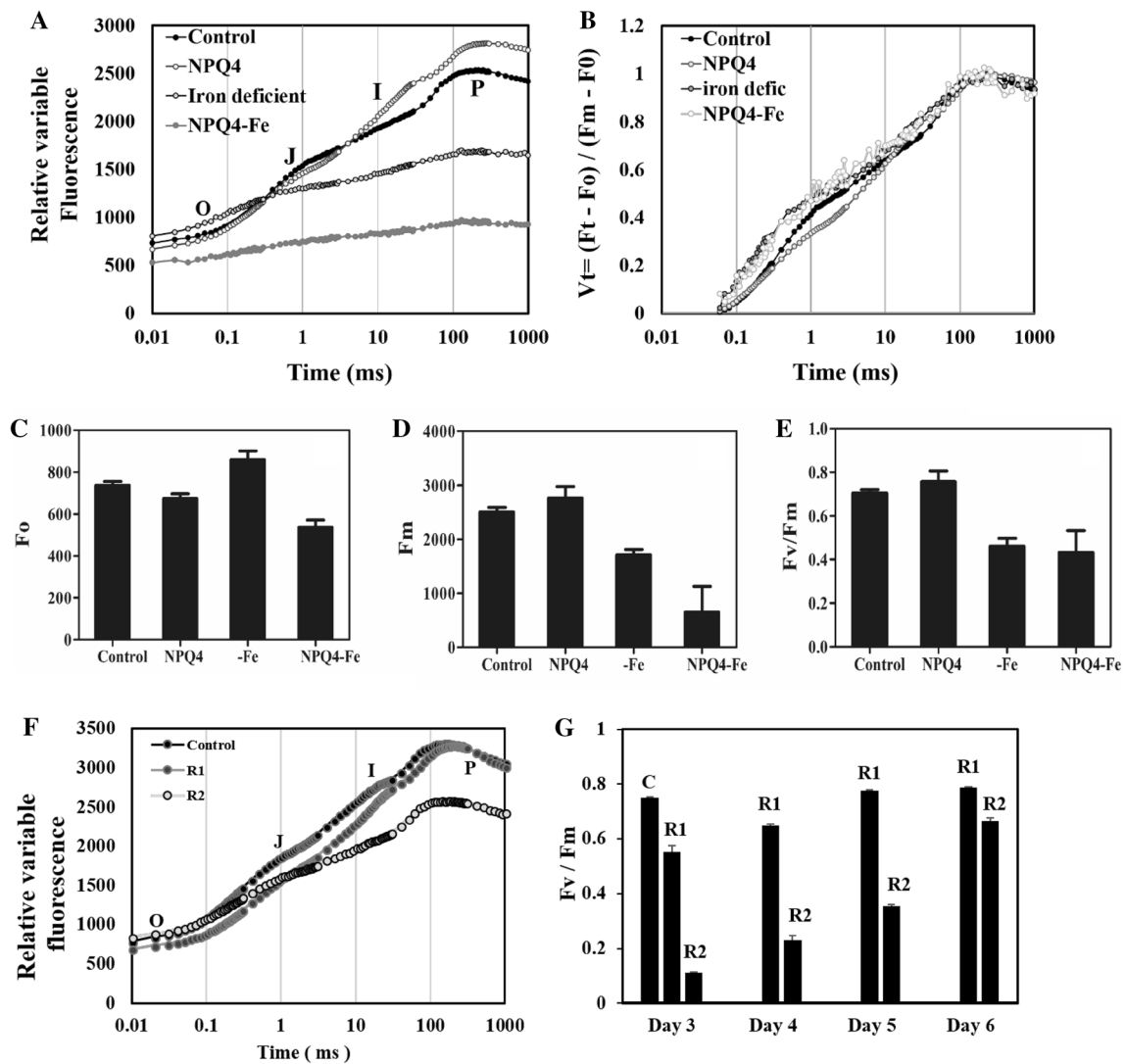


Fig. 1 **a** Chl *a* fluorescence transient (OJIP) curves from cultures of *wt* and *npq4* mutant *C. reinhardtii* grown in iron-sufficient control (+Fe) medium or iron-deficient (-Fe) medium; **b** double normalized values of OJIP curves; **c** F_o values; **d** F_m values; **e** F_v/F_m; **f** shows Chl *a* fluorescence transients (OJIP) curves from control, recovery

first (R1) cells, recovery second (R2) cells; **g** shows the F_v/f_m value from control (c), recovery first (R1), recovery second (R2). All samples were excited at 650 nm with 3000 μmol photons m⁻² s⁻¹ light. The measurements were repeated three times using different individual cultures

with increasing light intensity (250 μmol photons m⁻² s⁻¹) in the iron-deprived cells. This indicates that the electron flow is altered in cells grown under iron-deficient conditions. In addition, PSII quantum efficiency [Y(II)] values in increasing light intensities were decreased in both the *wt* and the *npq4* mutant under iron-deficiency compared with the iron-sufficient control (Fig. 2b). The first generation recovery of ETR and Y(II) values was reached to the control level after 4 days, whereas in second generation the recovery was after 6–7 days (Supplementary Fig. 3). This is due to changes in the redox state of the primary electron-accepting plastoquinone of the PSII centre in Fe-deficient conditions. Furthermore, compared with the control cultures, NPQ increased with rising light intensities in *wt*

cells, and to a lesser extent *npq4* cells grown under iron deficiency (Fig. 2c). Alterations in the PQ pool in iron-deficient cells could be attributed to the failure of PSI to draw electrons out of the pool or the activation of a mechanism to increase electron flow into the pool. Taken together, these results suggest that NPQ4/LHCSR3 modulates photosynthetic acclimation to iron-deficient conditions in *C. reinhardtii*.

Lipid accumulation observed by confocal microscopy

The accumulation of lipid bodies under iron-deprived conditions was examined by confocal microscopy (Fig. 3a).

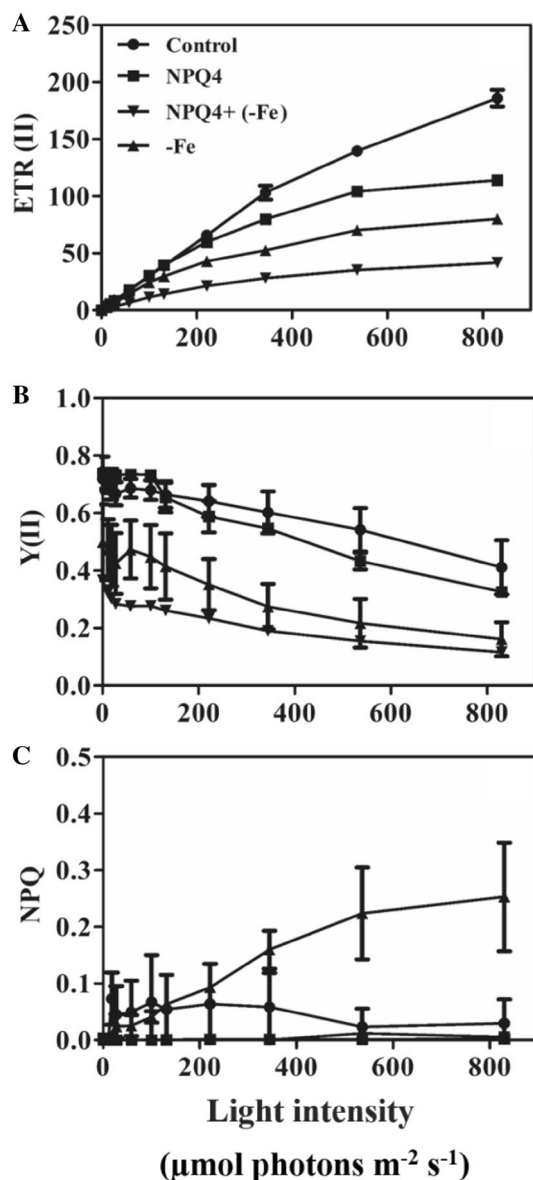


Fig. 2 Cells grown in iron-deficient (–Fe) conditions shows decreased photosynthetic electron flow compared to those grown with sufficient iron (+Fe). **a** Irradiance dependence of relative electron transport through PSII (ETR); **b** quantum yield of PSII Y(II); **c** non-photochemical quenching (NPQ) values for *wt* and *npq4* mutant cells grown in control (+Fe) and iron-deficient (–Fe) medium. The values are the means \pm SD from three independent experiments

Iron-deficient cells were half the normal size, displayed an abnormal morphology and a reduced chlorophyll content (data not shown). Lipid body production was clearly induced within 48 h of transfer to TAP – Fe medium and the cells accumulated a considerable number of lipid bodies. In contrast, cells grown in iron replete medium did not show any visible accumulation of lipid bodies. Thus, Fe deficiency caused *C. reinhardtii* cells to synthesize

additional lipids. The lipid accumulation in recovery cells was the same like in control (data not shown).

Identification of neutral lipids by Nile Red fluorescence

The neutral lipid content of cells during the growth of cultures for 4 days in control or iron-deficient conditions was determined by staining with Nile Red and measuring fluorescence (Fig. 4). Nile Red fluorescence has previously been shown to be proportional to the level of neutral lipid and cell density (Chen et al. 2009, 2011). After staining, numerous fluorescent lipid droplets (LDs) were observed in iron-deprived cells, but none or only a few were present in control cells (Fig. 3b). The LDs were highly fluorescent when viewed using the FITC filter set and were clearly distinguishable from the large chloroplast. A time course experiment using a TECAN fluorescence spectrophotometer revealed that the formation of LDs occurred within 48 h of transferring cells to iron-deficient medium, as gauged by the increase in Nile Red fluorescence (Fig. 4a). However, this was accompanied by a reduction in the optical density at 750 nm, a parameter indicative of cell growth. This OD_{750} value (0.395 ± 0.05) was around half that of the culture grown in control iron-sufficient conditions (0.822 ± 0.10), suggesting growth inhibition and a consequent decline in biomass. Overall, iron-deficient cells exhibited a fourfold increase in their neutral lipid content over the course of 4 days. For analysis of lipids, we restrict to the *wt* since the effect of Fe deficiency was more in *npq4* mutant.

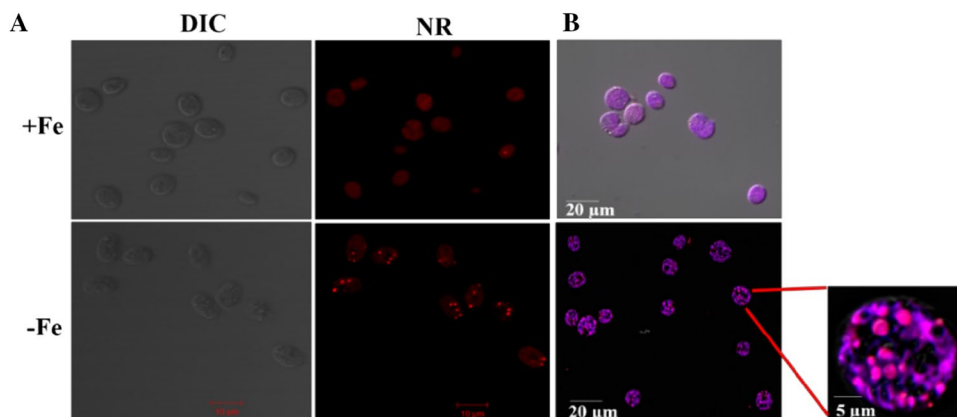
Analysis of neutral lipids by FACS

Neutral lipid accumulation in cells grown for 4 days in iron-sufficient (+Fe) and -deficient (–Fe) conditions was monitored by Nile Red staining and flow cytometry. Significant amounts of neutral lipids were accumulated in iron-deprived cells (mean fluorescence value, 29.27 ± 0.93) compared to control cells (7.293 ± 1.09) (Fig. 4b, c). These results demonstrate that the metabolism of iron and carbon in *C. reinhardtii* is interlinked, so that under conditions of iron deficiency a greater proportion of carbon fixed by photosynthesis (i.e. the output of the Calvin–Benson cycle) is channelled to produce neutral lipids (Velmurugan et al. 2014).

Impact of iron deprivation on photosynthetic proteins

The *C. reinhardtii* stress response protein LHCSR3 is important for energy-dependent quenching (qE), and its expression is induced under high light conditions that up-regulate qE (Peers et al. 2009; Bonente et al. 2011). *C. reinhardtii* has three genes for LHCSR3 isoforms (*lhcsr1*, *lhcsr 3.1*, and

Fig. 3 Lipid accumulation in *C. reinhardtii* cells examined by Nile Red staining and confocal microscopy. **a** Lipid droplets detected by fluorescence microscopy. Scale bar, 20 μ M. DIC differential interference contrast, scale bar 10 μ M; the images are representative of three independent replicates. **b** Formation of lipid droplets in cells exposed to 4 days of iron starvation



lhcsr 3.2), but *lhcsr 3.1* and *lhcsr 3.2* encode the same 259-amino acid polypeptide (Merchant et al. 2007). The LHCSR1 isoform has 253 residues with 87% sequence similarity to LHCSR3.1/LHCSR3.2. LHCSR3 expression is induced by low pH, the trigger of non-photochemical quenching. Surprisingly, we found that levels of this protein were increased in Fe-deficient cells. These results are consistent with the increase of NPQ fluorescence in wt and decrease in the *npq4* mutant (Fig. 3). Furthermore, we observed marginal changes in the levels of both RUBISCO subunits (SSU). As expected, and in agreement with the Chl *a* fluorescence data (Figs. 2, 3), the levels of the photosynthetic reaction centre proteins *psaA* (PSI) and *D1* (PSII) were significantly reduced under Fe-deficient conditions, which indicates decreased photosynthesis (Fig. 5a).

Impact of iron deprivation on fatty acid metabolism

Following the observation that iron starvation resulted in TAG accumulation and changes in FA levels, we examined levels of two key enzymes involved in lipid synthesis in *C. reinhardtii*. Phospholipid:diacylglycerol acyltransferase (PDAT1) (Boyle et al. 2012) is an enzyme that catalyses TAG synthesis via two pathways: transacylation of diacylglycerol with acyl groups from phospholipids and galactolipids, and DAG:DAG transacylation (Yoon et al. 2012; Kobayashi et al. 2013). Another enzyme, diacylglycerol acyl-transferase (DGAT2A) (Boyle et al. 2012), contributes to the incorporation of hydroxylated fatty acids into TAG (Zhang et al. 2009). There are six genes encoding DGAT in *Chlamydomonas* and previous studies have shown that the expression of DGAT2A is increased in nitrogen-starved cells (Boyle et al. 2012). We analysed DGAT2A and PDAT1 protein levels by western blotting using histone H3 as a control. After 72 h of growth in iron-deprived conditions the level of both enzymes was increased, although the expression of DGAT was lower than that of PDAT1.

Chlamydomonas reinhardtii under nitrogen-deficient conditions show an increase in the number of lipid droplets in

the cell (Kropat et al. 2011), which indicates that TAG are accumulated as an energy source in times of nutrient stress. Above we demonstrate that this also occurs in conditions of iron deficiency. In primitive and higher plants, intracellular neutral (TAG) storage lipid droplets (LD) are stabilized by a surface layer of phospholipids and a structural protein oleosin. Oleosins have proven difficult to detect in chlorophytes (green algae) (Huang et al. 2013) and the predominant protein associated with LD is termed the major lipid-droplet protein (MLDP). Immunoblot analysis using a MLDP-specific antibody showed increased levels of this protein in cells grown under iron-deprived conditions (Fig. 5c). Taken together, these results confirm that *C. reinhardtii* produces increased levels of neutral lipids that are stored in LD under iron-deficient conditions.

Quantification of total lipids by TLC

Biomass production occurs via a series of highly coordinated cellular processes, starting with the capture of light by photosystems, followed by the fixation of CO₂ through the Calvin–Benson cycle, and resulting in cell growth and division. In comparison with growth in iron-sufficient conditions, we observed a twofold decrease in total biomass in cells subjected to iron starvation (Fig. 6a). To characterize the overall change in lipid content caused by iron deficiency, we prepared a neutral lipid extract from equal dry weights of cells cultured on both control and Fe-depleted medium, and these were analysed by TLC. The TAG concentration was quantified based on a standard applied to the same TLC plates. The analysis of lipid samples from cells collected on each day of culture showed that the TAG content was increased significantly by Fe deficiency (Fig. 6b), although there was no change in polar lipid content.

Identification and quantification of fatty acids

The fatty acids of *C. reinhardtii* grown under control or iron-deficient conditions were extracted, converted to fatty

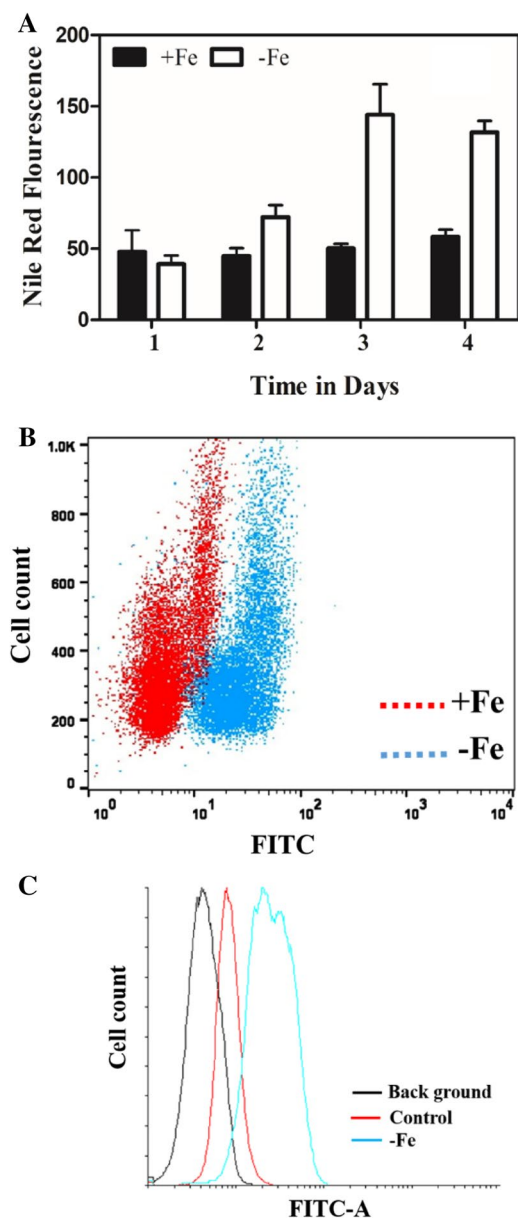


Fig. 4 Neutral lipid content of *C. reinhardtii* evaluated by Nile Red fluorescence. **a** Cultures grown in control (+Fe) and iron-deficient (–Fe) medium stained with Nile Red on days 1–4, then examined using a plate reader fluorometer. **b** FACS-two-dimensional dot plots of iron-deficient culture: unstained (red), Nile Red-stained (blue). **c** Histogram plot for iron-deficient unstained cells (background, black line), and iron-sufficient (red line) and iron-deficient cells stained with Nile Red (blue line). Statistical analysis of the median FITC-A values is presented

acid methyl esters (FAMES) by methylation with diazomethane and then identified and quantified by GC/MS (Lewis et al. 2000) (Table 1). The FAME mass spectra (GC-EIMS) were compared with those from the lipid library (NIST-Wiley library) to identify individual fatty acids, and heptadecanoic acid (17:0) was used as an internal standard for

quantification. Under conditions of iron deficiency, the cells were found to contain up to 50% fatty acids by total dry weight. The major fatty acids in these iron-depleted cells were 14:0, 16:0, 18:0, 18:2 and 18:3^{Δ9, 12, 15}. In addition, some essential fatty acids were identified including omega-3 and α linolenic fatty acids. Although TLC analysis of lipids showed an increased TAG content in iron-deficient cells (48–72 h) (Fig. 6b), there was no change in the total FA content. This may be due to recycling of membrane fatty acids into neutral lipid stores. FAME analysis of total fatty acids showed a marginal change in saturated FAs (e.g. 16:0 and 18:2) and interestingly levels of 18:0 were altered slightly, suggesting a distinct effect on membrane lipids. These results indicate that iron deficiency in *C. reinhardtii* leads to an altered FA profile and the accumulation of TAG. Essential fatty acids like omega-3, α -linolenic acid (18:3^{Δ9, 12, 15}), linoleic acid (18:2^{Δ9, 12}) and the omega-9 fatty acid oleic acid (18:1^{Δ9}) were identified but their level was not altered significantly in comparison to iron-sufficient condition.

The overall proportion of unsaturated fatty acids remained the same in both control (iron sufficient) and iron-depleted cells ($\Sigma\text{UNSAT}/\Sigma\text{FAME}=0.14\text{--}0.12$) (Table 1). Notably, the following fatty acids were not identified in cells cultured in either condition: 16:1^{Δ3}, 16:3^{Δ4,7,10}, 18:3^{Δ6,9,12} or 18:3^{Δ5,12,15}.

Discussion

In this study, we investigated the impact of iron deficiency on photosynthesis and lipid droplet formation in *C. reinhardtii* grown under photoheterotrophic conditions. Previously, we reported that the photosynthetic yield of PSI and PSII was reduced equally in *C. reinhardtii* subjected to iron deficiency (Yadavalli et al. 2012a; Devadasu et al. 2016). However, the damage to PSI function was more severe since PSI reaction centre assembly and electron transport require more Fe. The abundance of several proteins is altered in iron-depleted cells, especially the PsaC, D and E subunits of PSI and also the LHCI subunits. These alterations are likely to disrupt the assembly of the PSI–LHCI supercomplexes and similar changes were observed in iron-deficient rice (Yadavalli et al. 2012a, b). Moreover, electron transport and PSII supercomplex organization were also disturbed under Fe-deprived conditions (Devadasu et al. 2016). Since iron is crucial for both PSI and PSII functions, Fe deficiency was accompanied by many changes in cell structure.

In the present study, a drastic reduction in the photosynthetic yield of PSII was detected in iron-depleted *C. reinhardtii* cells. The yield was further decreased in a *npq4* mutant lacking the activity of a light-harvesting stress-related gene (Fig. 3). The pronounced increase in Fo and decline in the I–P phase of fluorescence induction that

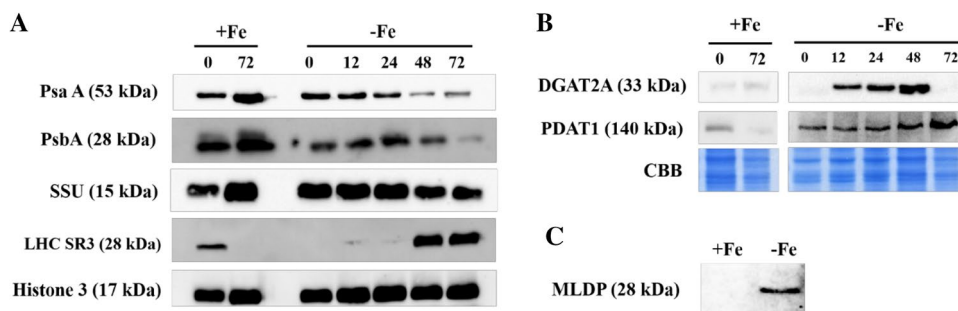
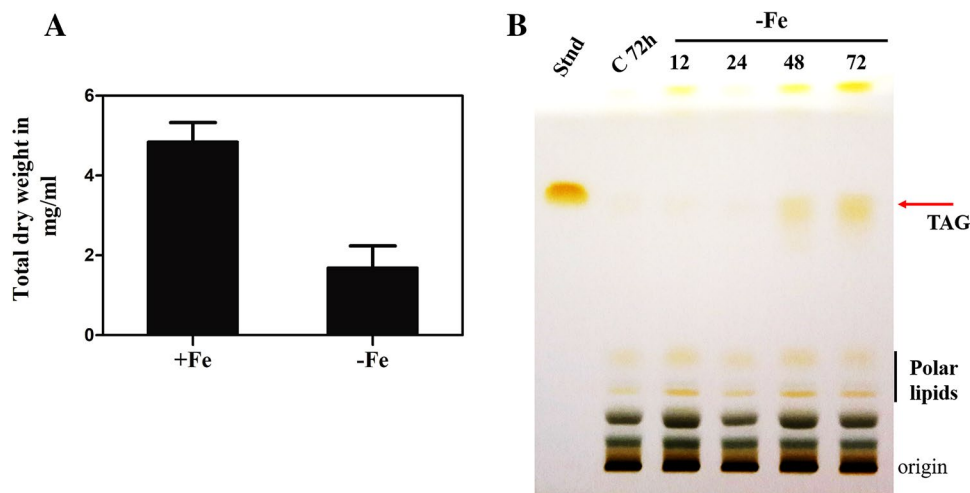


Fig. 5 Effect of iron deficiency on *C. reinhardtii* protein abundance monitored by western blotting. **a** For photosynthetic polypeptides, soluble or membrane protein extracts (20 μ g protein/lane) were separated by denaturing gel electrophoresis, transferred to PVDF or nitrocellulose membranes, and probed with specific antibodies for the indicated proteins. Histone H3 was used as a loading control. **b** West-

ern blot analysis of DGAT2A (Acyl-CoA:diacylglycerol acyltransferase) and phospholipid:diacylglycerol acyltransferase 1 (PDAT1) from cells grown for 0–72 h in iron-deficient conditions. Protein extracts (10 μ g protein/lane) were resolved on denaturing 10% Bis-Tris gels and equal loading was confirmed by CBB staining. **c** MLDP protein level in cells grown under iron-deficient conditions

Fig. 6 Lipid production by *C. reinhardtii* cells grown in control (+Fe) and iron-deficient (-Fe) conditions. **a** Cell biomass in the analysed cultures. **b** TLC analysis showing TAG accumulation caused by iron deficiency. Lipids extracted from cells were resolved on TLC plates and TAG were visualized by brief iodine staining. Triolein (5 μ g) was applied as a standard



reduced Fv/Fm and Fm indicate an impact on the electron transport chain (Fig. 2). An increase in Fo is a recognized effect of abiotic stress related to formation of inactive PSII centers or the dissociation of LHCII from the PSII core (Aro et al. 1993). Increased Fo in the dark Chl fluorescence could also result from a reduction in the PQ pool (Cournac et al. 2002). As observed in our previous study (Devadasu et al. 2016), the change in electron transport and quantum yield could indicate some alteration in reaction center proteins and PSII antenna proteins such as CP43 and 47. As expected, the second generation of Fe deficiency cells diminished the photosynthetic activity. However, the recovery of these cells has taken longer duration (6–7 days) indicating that these cells were in severe nutrient shock. Though the cells were alive, the cell division and restoration of photosynthetic activity took longer time as Fe deficiency results in multiple changes in the cell. In-depth studies are required to elucidate the mechanism that trigger the recovery process after iron starvation. As anticipated, the non-photochemical

change was increased in wild-type cells grown in Fe-deficient medium and unsurprisingly there was no alteration in NPQ in the *npq4* mutant (Figs. 2, 3). Notably, the expression of the LHCSR3 protein was significantly induced under Fe stress conditions (Fig. 5a). This change is in line with the finding that plants experiencing stress adapt or are protected by changes that increase heat dissipation from their photosynthetic apparatus. These changes include the increased expression of specific proteins (i.e. LHCSR3 in *C. reinhardtii* and PsbS in higher plants) that bind to Chl and carotenoids. Although cells subjected to iron-deficiency can generate a thylakoid lumen pH that is sufficiently acidic to induce the xanthophyll cycle, this stress decreases the capacity of photosynthetic electron transport so that it is unable to maintain a lumen pH acidic enough to induce NPQ and increase heat dissipation. It was reported earlier that energy-dependent quenching (qE) mechanism in algae is significantly different from that of higher plants due to the absence of PsbS (Bonente et al. 2011), whereas it has been recently

Table 1 Free fatty acid composition of *C. reinhardtii* cells grown under TAP + Fe for 72 h and TAP – Fe medium for 1–4 days

| FFA | TAP + Fe | TAP – Fe | | | |
|-----------------------------|----------|----------|--------|---------|--------|
| | C 72 h | 1 Day | 2 Day | 3 Day | 4 Day |
| C14:0 | 1.6026 | 0.4599 | 0.5037 | 1.6257 | 1.3714 |
| C15:0 | 0.1255 | 2.9210 | 0.1320 | 0.1076 | 0.1029 |
| C16:0 | 4.2757 | 3.8739 | 3.9251 | 4.1763 | 3.8728 |
| C16:1 ^{Δ9} | 0.0052 | 0.0065 | 0.0012 | 0.0020 | 0.0017 |
| C16:1 ^{Δ11} | 0.0902 | 0.0157 | 0.0119 | 0.0209 | 0.0102 |
| C16:2 ^{Δ7,10} | 0.0114 | 0.0064 | 0.0077 | 0.0102 | 0.0094 |
| C16:3 ^{Δ7,10,13} | 0.0663 | 0.0309 | 0.0320 | 0.0399 | 0.0302 |
| C16:4 ^{Δ4,7,10,13} | 0.1733 | 0.1046 | 0.0838 | 0.1462 | 0.0981 |
| C18:0 | 3.2601 | 3.2311 | 3.3319 | 3.2809 | 3.2484 |
| C18:1 ^{Δ9 or 11} | 0.0748 | 0.0466 | 0.0403 | 0.0464 | 0.0434 |
| C18:2 ^{Δ9,12} | 0.0955 | 0.0837 | 0.0959 | 0.1390 | 0.1239 |
| C18:3 ^{Δ5,9,12} | 0.0351 | 0.0300 | 0.0302 | 0.0584 | 0.0526 |
| C18:3 ^{Δ9,12,15} | 0.0093 | 0.0049 | 0.0038 | 0.0090 | 0.0086 |
| C18:3 | 0.5779 | 0.3418 | 0.3106 | 0.3888 | 0.4151 |
| C20:0 | 0.0354 | 0.0355 | 0.0352 | 0.0334 | 0.0380 |
| C22:0 | 0.0038 | 0.0036 | 0.0040 | 0.0028 | 0.0036 |
| C22:1 ^{Δ13} | 0.0117 | 0.0129 | 0.0112 | 0.0084 | 0.0101 |
| Total FAME | 10.8537 | 8.8048 | 8.9608 | 10.4959 | 9.8403 |
| ∑SAT | 9.3031 | 7.7209 | 7.9320 | 9.2267 | 8.6371 |
| ∑MONO | 0.1818 | 0.0817 | 0.0647 | 0.0777 | 0.0654 |
| ∑POLY | 0.9688 | 0.6023 | 0.5641 | 0.7915 | 0.7379 |
| ∑UNSAT | 1.5506 | 1.0840 | 1.0288 | 1.2692 | 1.2032 |
| ∑UNSAT/FAME | 0.142 | 0.123 | 0.114 | 0.120 | 0.122 |

reported that PsbS protein is transiently expressed in *C. reinhardtii* and is essential for the activation of non-photochemical quenching. It indicated that PsbS protein could be promoting conformational changes required for the activation of LHCSR3-dependent quenching in the antenna of PS II (Correa-Galvis et al. 2016). Hence, this protein LHCSR3 or Lhc gene compound called LHCSR3 (formerly known as LI818) is essential for qE. Of the three LhcsR isoforms present in *C. reinhardtii*, LHCSR3 is the only one responsive at low pH, the trigger of non-photochemical quenching. Upon acidification under high light conditions, the energy dissipation properties of this protein are increased (Bonente et al. 2011). LHCSR3 expression is characteristic of high light stress conditions, so it was surprising to find that iron deficiency also induces the production of this protein. Thus, it is apparent that the increase in non-photochemical quenching occurring in Fe stress conditions causes an increase in LHCSR3 expression that is similar to that under high light stress conditions.

Taken together, the results of this study show that carbon fixation is the preferred bioenergetic pathway in *Chlamydomonas*. These photoheterotrophic cells, given the option to grow heterotrophically, suppressed the expression

of iron-containing photosynthetic proteins (PsaA and PsbA) in response to iron-deficient conditions, but no significant changes in the level of Rubisco large and small subunit proteins were observed.

When grown under iron-starvation conditions, *C. reinhardtii* cells displayed an abnormal morphology and tended to form clumps (Fig. 1). These multicellular aggregates resemble palmelloids that are observed in salt stress condition (Neelam and Subramanyam 2013). In addition, the growth rate of the iron-limited photoheterotrophic cells was severely decreased. It is interesting that although the photosynthetic efficiency decreased, lipid droplet accumulation was increased by Fe stress. Earlier reports noted increased lipid droplet formation in *C. reinhardtii* grown under conditions of nitrogen deficiency (Nguyen et al. 2011). During photoheterotrophic growth, the carbon is fixed into cellular biomass, which would explain why more lipid droplets are produced by these cells than by those employing photosynthesis (Ravenel 1988). The increase of lipid accumulation can be a result of imbalance between photosynthetic efficiency and utilization of assimilates under Fe deficiency and this could be one of the reasons to slow-down the biomass production. Thus, we assume that the photosynthesis seems to be not the primary reason of the lower biomass production in conditions of iron deficiency.

MLDP is a protein specific to algae that was identified in a previous study as being induced by nitrogen deficiency and associated with lipid droplets in *C. reinhardtii* (Huang et al. 2013). MLDP appears to have a structural role, but its specific molecular and biochemical functions remain uncharacterized. We found that MLDP expression is highly induced in response to iron deprivation, and its abundance correlates with the number and size of lipid droplets produced, supporting a role for this protein in their formation.

Chlamydomonas reinhardtii cells completely deprived of iron also contained more saturated FA. Since TAG is naturally more abundant in saturated FA, the accumulation of TAG under iron starvation conditions might account for this increase in saturated FA (Urzica et al. 2013). Iron-depleted cells showed a slight increase in the most abundant FA, C16:0 (Table 1). However, the total FA content in *C. reinhardtii* remained relatively stable in iron-deficient conditions, indicating that another mechanism is responsible for the elevated content of saturated FA. A shift from highly polyunsaturated species to less unsaturated FAs has been observed under several stress conditions as a protective mechanism. Polyunsaturated FAs are major components of photosynthetic membranes that are prone to oxidation under Fe stress conditions, and this could cause a loss of photosynthetic activity. A similar phenomenon was observed in *C. reinhardtii* subjected to different abiotic stresses (Nguyen et al. 2013). The rate of lipid oxidation might be reduced in cells containing low levels of polyunsaturated FAs, making

them more tolerant of stress conditions. Acyltransferases responsible for de novo TAG biosynthesis (type 1 DGAT1 or type 2 DGTs) in *C. reinhardtii* were previously identified based on homology to *A. thaliana* (DGAT1 and DGAT2) and yeast (ARE1, ARE2, and DGA1, respectively) enzymes (Yoon et al. 2012). PDAT1 and DGAT1 of *A. thaliana* are both involved in seed oil accumulation (Zhang et al. 2009). In the present study, we found that *C. reinhardtii* PDAT1 and DGAT2A show greatly increased expression upon iron starvation that is associated with lipid droplet formation, which strongly supports a role for these enzymes in TAG accumulation.

Iron starvation affects the expression of PDAT1 and DGAT2A in a similar manner to nitrogen starvation with the abundance of both enzymes increasing considerably after 48–72 h of iron deficiency condition (Fig. 5b). Iron deficiency-induced TAG synthesis pathway is dependent on both acyl-CoA-dependent and -independent acyltransferases (Yoon et al. 2012). Our data corroborate a previous report that PDAT1 from *C. reinhardtii* mediates lipid turnover by using its hydrolase activity to catabolize galactolipids and phospholipids for TAG synthesis. In cyanobacteria, *Synechococcus* sp. PCC7942, the thylakoids lipids which are PG, MGDG and DGDG were reduced in order to maintain the dynamics of membrane (Ivanov et al. 2007). However, little is known about the TAG accumulation during iron starvation.

Fully iron-deprived *C. reinhardtii* cells contain raised levels of saturated FA. Because TAG is naturally rich in 16:0 and 18:0 FA, TAG accumulation might account for the increase in saturated FA. However, our data demonstrate that the total FA content in *C. reinhardtii* cells remains relatively stable under iron-deficient conditions. This indicates that another mechanism is responsible for the elevated content of saturated FA, which leads to TGA accumulation (Table 1). Furthermore, the expression of both Rubisco subunits was unchanged in iron-deprived cells (Fig. 5a), which indicates that a coordinated process, dependent on the capture of light by the photosystems and fixation of CO₂ via the Calvin–Benson cycle, is responsible for the increased TAG biosynthesis.

In conclusion, the results of this study confirm that iron deficiency induces the formation of lipid droplets, since the photosynthetic parameters and lipid profiles studied are similar to the control (Petroustos et al. 2009). However, the iron-depleted cells show different photosynthetic phenotypes, as revealed by the notable reduction in Fv/Fm during the experiment indicative of a lowering of both the effective quantum yield of photosystem II (Φ PSII) and the photosynthetic capacity (ETR) when compared with the control. Taken together, the findings of this study suggest the existence of complex feedback interactions between the Rubisco enzyme and carbon fixation in *C. reinhardtii* and should help inform strategies for tuning carbon metabolism toward lipid

biosynthesis and altered lipid composition. Importantly, the expression of light-harvesting stress protein LHCSR3 under Fe deficiency conditions indicate that non-photochemical quenching prevails in order to photo-protect. Furthermore, our results indicate that cells grown under iron-deficient conditions could be useful for biodiesel production because they show an increase in lipid content, and especially neutral lipids over polar lipids. Furthermore, the lipid composition of iron-deprived cell indicates a reduced content of unsaturated FAs, which is another desirable characteristic for biodiesel production.

Acknowledgements R.S was supported by the Council of Scientific and Industrial Research [No. 38(1279)/11/EMR-II and No. 38(1381)/14/EMR-II], Department of Biotechnology (BT/PR14964/BPA/118/137/2015) and DST-FIST, UGC-SAP, Govt. of India, for financial support. ED acknowledges the receipt of a UGC-RGNF fellowship. We thank Anthony H. C. Huang for the antibody against MLDP. We acknowledge Dr. John R. Gittins, University of Southampton, National Oceanography Center, Waterfront Road, Southampton, UK for his critical reading and also English correction.

Compliance with ethical standards

Conflict of interest The authors declare that they have no conflict of interest.

References

- Andaluz S, Millan AF, De las Rivas J, Aro EM, Abadía J (2006) Proteomic profiles of thylakoid membranes and changes in response to iron deficiency. *Photosynth Res* 89:141–155
- Aro EM, Virgin I, Andersson B (1993) Photoinhibition of photosystem II. Inactivation, protein damage and turnover. *Biochim Biophys Acta* 1143:113–134
- BenMoussa-Dahmen I, Chtourou H, Rezgui F, Sayadi S, Dhoubi A (2016) Salinity stress increases lipid, secondary metabolites and enzyme activity in *Amphora subtropica* and *Dunaliella* sp. for biodiesel production. *Bioresour Technol* 218:816–825
- Bibby TS, Nield J, Barber J (2001) Iron deficiency induces the formation of an antenna ring around trimeric photosystem I in cyanobacteria. *Nature* 412:743–745
- Boekema EJ, Hifney A, Yakushevskaya AE, Piotrowski M, Keegstra W, Berry S, Michel KP, Pistorius EK, Kruijff J (2001) A giant chlorophyll-protein complex induced by iron deficiency in cyanobacteria. *Nature* 412:745–753
- Bonente G, Ballottari M, Truong TB, Morosinotto T, Ahn TK, Fleming GR, Niyogi KK, Bassi R (2011) Analysis of LHCSR3, a protein essential for feedback de-excitation in the green alga *Chlamydomonas reinhardtii*. *PLoS Biol* 9:e1000577
- Borowitzka MA, Moheimani NR (2013) Sustainable biofuels from algae. *Mitig Adapt Strateg Global Change* 18:13–25
- Boyle NR, Page MD, Liu B, Blaby IK, Casero D, Kropat J, Cokus SJ, Hong-Hermesdorf A, Shaw J, Karpowicz SJ (2012) Three acyltransferases and nitrogen-responsive regulator are implicated in nitrogen starvation-induced triacylglycerol accumulation in *Chlamydomonas*. *J Biol Chem* 287:15811–15825
- Busch A, Rimbau B, Naumann B, Rensch S, Hippler M (2008) Ferritin is required for rapid remodeling of the photosynthetic

- apparatus and minimizes photo-oxidative stress in response to iron availability in *Chlamydomonas reinhardtii*. *Plant J* 55:201–211
- Cakmak ZE, Olmez TT, Cakmak T, Menemen Y, Tekinay T (2014) Induction of triacylglycerol production in *Chlamydomonas reinhardtii*: comparative analysis of different element regimes. *Biores Technol* 155:379–387
- Chauhan D, Folea IM, Jolley CC, Kouril R, Lubner CE, Lin S, Kolber D, Wolfe-Simon F, Golbeck JH, Boekema EJ, Fromme P (2011) A novel photosynthetic strategy for adaptation to low-iron aquatic environments. *Biochemistry* 50:686–692
- Chen W, Zhang C, Song L, Sommerfeld M, Hu Q (2009) A high throughput Nile red method for quantitative measurement of neutral lipids in microalgae. *J Microbiol Methods* 77:41–47
- Chen M, Tang H, Ma H, Holland TC, Ng KYS, Salley SO (2011) Effect of nutrients on growth and lipid accumulation in the green algae *Dunaliella tertiolecta*. *Biores Technol* 102:1649–1655
- Chen L, Ding C, Zhao X, Xu J, Mohammad AA, Wang S, Ding Y (2015) Differential regulation of proteins in rice (*Oryza sativa* L.) under iron deficiency. *Plant Cell Rep* 34:83–96
- Chisti Y (2007) Biodiesel from microalgae. *Biotechnol Adv* 25:294–306
- Correa-Galvis V, Redekop P, Guan K, Griess A, Truong TB, Wakao S, Niyogi KK, Jahns P (2016) Photosystem II subunit PsbS is involved in the induction of LHCSR protein-dependent energy dissipation in *Chlamydomonas reinhardtii*. *J Biol Chem* 291:17478–17565
- Cournac L, Latouche G, Cerovic Z, Redding K, Ravenel J, Peltier G (2002) In vivo interactions between photosynthesis, mitorespiration, and chlororespiration in *Chlamydomonas reinhardtii*. *Plant Physiol* 129:1921–1929
- Devadasu ER, Madireddi SK, Nama S, Subramanyam R (2016) Iron deficiency cause changes in photochemistry, thylakoid organization, and accumulation of photosystem II proteins in *Chlamydomonas reinhardtii*. *Photosynth Res* 130:469–478
- Fan J, Andre C, Xu C (2011) A chloroplast pathway for the de novo biosynthesis of triacylglycerol in *Chlamydomonas reinhardtii*. *FEBS Lett* 585:1985–1991
- Glaesener AG, Merchant SS, Blaby-Haas CE (2013) Iron economy in *Chlamydomonas reinhardtii*. *Front Plant Sci* 4:337–349
- Huang NL, Huang MD, Chen TL, Huang AH (2013) Oleosin of subcellular lipid droplets evolved in green algae. *Plant Physiol* 161:1862–1874
- Ivanov AG, Krol M, Sveshnikov D, Selstam E, Sandström S, Koochek M, Park Y, Vasil'ev S, Bruce D, Öquist G, Huner NPA (2006) Iron deficiency in cyanobacteria causes monomerization of photosystem I trimers and reduces the capacity for state transitions and the effective absorption cross section of photosystem I in vivo. *Plant Physiol* 141:1436–1445
- Ivanov AG, Krol M, Sveshnikov D, Selstam E, Sane PV, Sveshnikov D, Park Y, Öquist G, Huner NPA (2007) The induction of CP43' by Iron-stress in *Synechococcus* sp. PCC 7942 associated with carotenoid accumulation and enhanced fatty acid unsaturation. *Biochim Biophys Acta* 1767:807–813
- James Gabriel O, Hocart Charles H, Hillier W, Chen H, Kordbacheh F, Price D, Djordjevic G, Michael A (2011) Fatty acid profiling of *Chlamydomonas reinhardtii* under nitrogen deprivation. *Biores Technol* 102:3343–3351
- Juergens MT, Deshpande RR, Lucker BF, Park JJ, Wang H, Gargouri M, Holguin FO, Disbrow B, Schaub T, Skepper JN, Kramer DM, Gang DR, Hicks LM, Shachar-Hill Y (2015) The regulation of photosynthetic structure and function during nitrogen deprivation in *Chlamydomonas reinhardtii*. *Plant Physiol* 167:558–631
- Kobayashi N, Noel EA, Barnes A, Rosenberg J, DiRusso C, Black P, Oyler GA (2013) Rapid detection and quantification of triacylglycerol by HPLC-ELSD in *Chlamydomonas reinhardtii* and *Chlorella* strains. *Lipids* 48:1035–1049
- Kodru S, Malavath T, Devadasu E, Nellaepalli S, Stirbet A, Subramanyam R, Govindjee (2015) The slow S to M rise of chlorophyll a fluorescence reflects transition from state 2 to state 1 in the green alga *Chlamydomonas reinhardtii*. *Photosynth Res* 125:219–231
- Kosourov S, Patrusheva E, Ghirardi L, Seibert M, Tsygankov A (2007) A comparison of hydrogen photoproduction by sulfur-deprived *Chlamydomonas reinhardtii* under different growth conditions. *J Biotechnol* 128:776–787
- Kropat J, Hong-Hermesdorf A, Casero D, Ent P, Castruita M, Pellegrini M, Merchant SS, Malasarn D (2011) A revised mineral nutrient supplement increases biomass and growth rate in *Chlamydomonas reinhardtii*. *Plant J* 66:770–780
- Lewis T, Nichols PD, McMeekin TA (2000) Evaluation of extraction methods for recovery of fatty acids from lipid-producing microheterotrophs. *J Microbiol Methods* 43:107–116
- Li X, Moellering ER, Liu B, Johnny C, Fedewa M, Sears BB, Kuo MH, Benning C (2012a) A galactoglycerolipid lipase is required for triacylglycerol accumulation and survival following nitrogen deprivation in *Chlamydomonas reinhardtii*. *Plant Cell* 24:4670–4686
- Li X, Benning C, Kuo MH (2012b) Rapid triacylglycerol turnover in *Chlamydomonas reinhardtii* requires a lipase with broad substrate specificity. *Eukaryot Cell* 11:1451–1462
- Merchant SS et al (2007) The *Chlamydomonas* genome reveals the evolution of key animal and plant functions. *Science* 318:245–250
- Moody JW, McGinty CM, Quinn JC (2014) Global evaluation of biofuel potential from microalgae. *Proc Natl Acad Sci USA* 111:8691–8697
- Moseley JL, Allinger T, Herzog S, Hoerth P, Wehinger E, Merchant S, Hippler M (2002) Adaptation to Fe-deficiency requires remodeling of the photosynthetic apparatus. *EMBO J* 21:6709–6720
- Msilini N, Zaghdoudi M, Govindachary S, Lachaa'l M, Ouerghi Z (2011) Inhibition of photosynthetic oxygen evolution and electron transfer from the quinone acceptor Q_A^- to Q_B by iron deficiency. *Photosynth Res* 107:247–256
- Naumann B, Stauber EJ, Busch A, Sommer F, Hippler M (2005) N-terminal processing of Lhca3 is a key step in remodeling of the photosystem I-light-harvesting complex under iron deficiency in *Chlamydomonas reinhardtii*. *J Biol Chem* 280:20431–20441
- Naumann B, Busch A, Allmer J, Ostendorf E, Zeller M, Kirchhoff H, Hippler M (2007) Comparative quantitative proteomics to investigate the remodeling of bioenergetic pathways under iron deficiency in *Chlamydomonas reinhardtii*. *Proteomics* 7:3964–3979
- Neelam S, Subramanyam R (2013) Alteration of photochemistry and protein degradation of photosystem II from *Chlamydomonas reinhardtii* under high salt grown cells. *J Photochem Photobiol B* 124:63–70
- Nguyen HM, Baudet M, Cuine S, Adriano JM, Barthe D, Billon E, Bruley C, Beisson F, Peltier G, Ferro M, Li-Beisson Y (2011) Proteomic profiling of oil bodies isolated from the unicellular green microalga *Chlamydomonas reinhardtii*: with focus on proteins involved in lipid metabolism. *Proteomics* 11:4266–4273
- Nguyen HM, Cuine S, Beyly-Adriano A, Legeret B, Billon E, Auroy P, Beisson F, Peltier G, Li-Beisson Y (2013) The green microalga *Chlamydomonas reinhardtii* has a single omega-3 fatty acid desaturase that localizes to the chloroplast and impacts both plastidic and extraplastidic membrane lipids. *Plant Physiol* 163:914–928
- Peers G, Truong TB, Ostendorf E, Busch A, Elrad D, Grossman AR, Hippler M, Niyogi KK (2009) An ancient light-harvesting protein is critical for the regulation of algal photosynthesis. *Nature* 462:518–521
- Petroussos D, Terauchi AM, Busch A, Hirschmann I, Merchant SS, Finazzi G, Hippler M (2009) PGRL1 participates in iron-induced remodeling of the photosynthetic apparatus and in energy metabolism in *Chlamydomonas reinhardtii*. *J Biol Chem* 284:32770–32781

- Porra RJ, Thompson WA, Kriedemann PE (1989) Determination of accurate extinction coefficients and simultaneous equations for assaying chlorophylls a and b extracted with four different solvents: verification of the concentration of chlorophyll standards by atomic absorption spectroscopy. *Biochim Biophys Acta* 975:384–394
- Ravenel JA (1988) The iron and molybdenum use efficiencies of plant growth with different energy, carbon and nitrogen sources. *New Phytol* 109:279–287
- Schansker G, Strasser RJ (2005) Quantification of non- Q_B -reducing centers in leaves using a far-red pre-illumination. *Photosynth Res* 84:145–151
- Stirbet A, Govindjee (2011) On the relation between the Kautsky effect (chlorophyll a fluorescence induction) and Photosystem II: basics and applications of the OJIP fluorescence transient. *J Photochem Photobiol B* 104:236–257
- Stirbet A, Govindjee (2012) Chlorophyll a fluorescence induction: understanding the thermal phase, the J-I-P rise. *Photosynth Res* 113:15–61
- Terauchi AM, Peers G, Kobayashi MC, Niyogi KK, Merchant SS (2010) Trophic status of *Chlamydomonas reinhardtii* influences the impact of iron deficiency on photosynthesis. *Photosynth Res* 105:39–49
- Timperio AM, D'Amici GM, Barta C, Loreto F, Zolla L (2007) Proteomics, pigment composition, and organization of thylakoid membranes in iron-deficient spinach leaves. *J Exp Bot* 58:3695–3710
- Towbin H, Staehelin T, Gordon J (1979) Electrophoretic transfer of proteins from polyacrylamide gels to nitrocellulose sheets: procedure and some applications. *Proc Natl Acad Sci USA* 76:4350–4354
- Urzica EI, Vieler A, Hong-Hermesdorf A, Page MD, Casero D, Gallaheer SD, Kropat J, Pellegrini M, Benning C, Merchant SS (2013) Remodeling of membrane lipids in iron-starved *Chlamydomonas*. *J Biol Chem* 288:30246–30258
- Velmurugan N, Sung M, Yim SS, Park MS, Yang JW, Jeong KJ (2014) Systematically programmed adaptive evolution reveals potential role of carbon and nitrogen pathways during lipid accumulation in *Chlamydomonas reinhardtii*. *Biotechnol Biofuel* 7:117–132
- Wellburn AR (1994) The spectral determination of chlorophylls a and b, as well as total carotenoids, using various solvents with spectrophotometers of different resolution. *J Plant Physiol* 144:307–313
- Yadavalli V, Jolley CC, Malleda C, Thangaraj B, Fromme P, Subramanyam R (2012a) Alteration of proteins and pigments influence the function of photosystem I under iron deficiency from *Chlamydomonas reinhardtii*. *PLoS ONE* 7:e35084
- Yadavalli V, Neelam S, Rao ASVC, Reddy AR, Subramanyam R (2012b) Differential degradation of photosystem I subunits under iron deficiency in rice. *J Plant Physiol* 169:753–759
- Yoon K, Han D, Li Y, Sommerfeld M, Hu Q (2012) Phospholipid:diacylglycerol acyltransferase is a multifunctional enzyme involved in membrane lipid turnover and degradation while synthesizing triacylglycerol in the unicellular green microalga *Chlamydomonas reinhardtii*. *Plant Cell* 24:3708–3724
- Zhang M, Fan J, Taylor DC, Ohlrogge JB (2009) DGAT1 and PDAT1 acyltransferases have overlapping functions in Arabidopsis triacylglycerol biosynthesis and are essential for normal pollen and seed development. *Plant Cell* 21:3885–3901